AD-A041 421 AIR FORCE MATERIALS LAB WRIGHT-PATTERSON AFB OHIO F/G 11/6
A STUDY OF CONSTITUENT, DISPERSOID, AND HARDENING PARTICLES IN --ETC(U)
MAR 77 J S SANTNER

UNCLASSIFIED AFML-TR-76-200 NL

| OF |
AD
A041421

END

DATE
FILMED
8-77

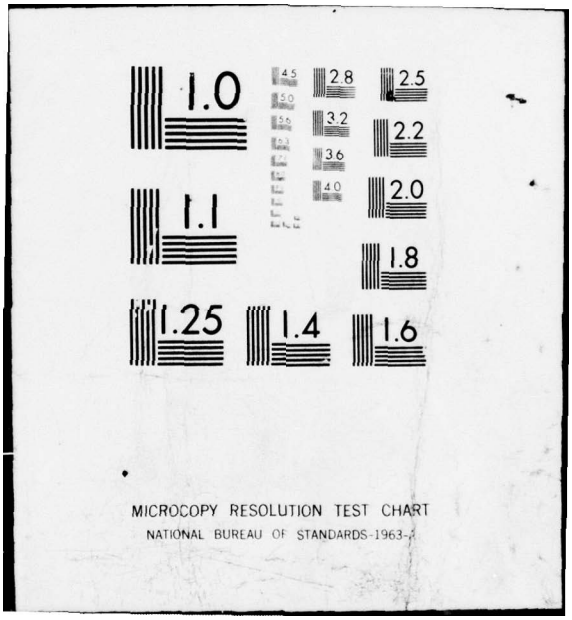
1.0
1.1
1.25
1.4
1.6
1.8
2.0
2.2
2.5
2.8
3.2
3.6
4.0
4.5
5.0
5.6
MICROCOPY RESOLUTION TEST CHART
NATIONAL BUREAU OF STANDARDS-1963-A

AFML-TR-76-200



# A STUDY OF CONSTITUENT, DISPERSOID, AND HARDENING PARTICLES IN THE FRACTURE OF 7075 ALUMINUM ALLOYS

*STRUCTURAL METALS BRANCH*
*METALS AND CERAMICS DIVISION*

MARCH 1977

TECHNICAL REPORT AFML-TR-76-200
FINAL REPORT FOR PERIOD JULY 1975 - FEBRUARY 1976







AIR FORCE MATERIALS LABORATORY
AIR FORCE WRIGHT AERONAUTICAL LABORATORIES
AIR FORCE SYSTEMS COMMAND
WRIGHT-PATTERSON AIR FORCE BASE, OHIO 45433

NOTICE

When Government drawings, specifications, or other data are used for any purpose other than in connection with a definitely related Government procurement operation, the United States Government thereby incurs no responsibility nor any obligation whatsoever; and the fact that the government may have formulated, furnished, or in any way supplied the said drawings, specifications, or other data, is not to be regarded by implication or otherwise as in any manner licensing the holder or any other person or corporation, or conveying any rights or permission to manufacture, use, or sell any patented invention that may in any way be related thereto.

This report has been reviewed by the Information Office (IO) and is releasable to the National Technical Information Service (NTIS). At NTIS, it will be available to the general public, including foreign nations.

This technical report has been reviewed and is approved for publication.

L. R. BIDWELL
Program Manager

FOR THE COMMANDER

N. G. TUPPER
Chief, Structural Metals Branch
Metals and Ceramics Division
Air Force Materials Laboratory

Copies of this report should not be returned unless return is required by security considerations, contractural obligations, or notice on a specific document.

UNCLASSIFIED

SECURITY CLASSIFICATION OF THIS PAGE (When Data Entered)

## REPORT DOCUMENTATION PAGE

READ INSTRUCTIONS BEFORE COMPLETING FORM

1. REPORT NUMBER: AFML-TR-76-200
2. GOVT ACCESSION NO.:
3. RECIPIENT'S CATALOG NUMBER:

4. TITLE (and Subtitle): A STUDY OF CONSTITUENT, DISPERSOID, AND HARDENING PARTICLES IN THE FRACTURE OF 7075 ALUMINUM ALLOYS

5. TYPE OF REPORT & PERIOD COVERED: Final report for period July 1975-February 1976

6. PERFORMING ORG. REPORT NUMBER:

7. AUTHOR(s): JOSEPH S. SANTNER

8. CONTRACT OR GRANT NUMBER(s):

9. PERFORMING ORGANIZATION NAME AND ADDRESS:
Air Force Materials Laboratory (LLS)
Air Force Wright Aeronautical Laboratories
Wright-Patterson AFB, OH 45433

10. PROGRAM ELEMENT, PROJECT, TASK AREA & WORK UNIT NUMBERS:
Project 2418
Task 241802
24180204
62102F

11. CONTROLLING OFFICE NAME AND ADDRESS:
Air Force Materials Laboratory (LLS)
Air Force Wright Aeronautical Laboratories
Wright Patterson AFB, OH 45433

12. REPORT DATE: March 1977

13. NUMBER OF PAGES: 46 pages

14. MONITORING AGENCY NAME & ADDRESS (if different from Controlling Office):

15. SECURITY CLASS. (of this report): Unclassified

15a. DECLASSIFICATION/DOWNGRADING SCHEDULE:

16. DISTRIBUTION STATEMENT (of this Report)
Approved for public release; distribution unlimited.

17. DISTRIBUTION STATEMENT (of the abstract entered in Block 20, if different from Report)



18. SUPPLEMENTARY NOTES
Submitted for Publication to Met. Trans.

19. KEY WORDS (Continue on reverse side if necessary and identify by block number)

| | | |
|---|---|---|
| Aluminum Alloy | Fracture Toughness | Thermomechanical Processing |
| Purity | Analysis of Variance | |
| Dispersoid Particles | Notch Tensile Test | |
| Heat Treatment | Zirconium | |

20. ABSTRACT (Continue on reverse side if necessary and identify by block number)

Ten different alloys based on the 7075 composition are used to study the effect of purity level, dispersoid type, and heat treatment on 7075's fracture toughness. Five different purity levels ranging from 0.03 w/o to 0.30 w/o Fe+Si and two different dispersoid types were investigated. Each alloy was given two different heat treatments with both the longitudinal and the long-transverse directions tested.

The notched round tensile test was modified to give the "plastic energy per unit area". This parameter used for ranking fracture toughness gave the same

DD FORM 1 JAN 73 1473 EDITION OF 1 NOV 65 IS OBSOLETE

UNCLASSIFIED

SECURITY CLASSIFICATION OF THIS PAGE (When Data Entered)

D12320

results as the total energy per unit area measured on precracked Charpy specimens. Moreover, the fracture toughness ranking for these ten alloys was the same in the longitudinal and long-transverse directions. This suggests the elongated distribution of constituent particles in the rolling direction does not change the failure mechanism. Fractographic evidence showed a clear difference in the fracture topography between the ten alloys.

An analysis of variance demonstrated that heat treatment was the most significant variable investigated that affects fracture toughness. This result supports a two-stage ductile fracture failure mechanism which suggests that the dispersoid and hardening particles are primarily responsible for the fracture toughness of the higher purity aluminum alloys used by the aerospace industry today.

## FOREWORD

The work described in this report was performed by the Structural Metals Branch, Metals and Ceramics Division, Air Force Materials Laboratory, Wright Aeronautical Laboratories, Air Force Systems Command, Wright-Patterson Air Force Base, Ohio. The Project Number was 2418, "Metallic Structural Materials", and the Task Number was 241802, "Metals and Alloys Technology". The research was conducted between July 1975 and February 1976.

The mechanical testing reported herein was conducted by Charles O. Smith while the fractographic investigation was conducted by Russel Pense and Ralph Omlor. The author wishes to thank Lawrence R. Bidwell for reviewing the original manuscript. The project engineer wishes to thank Joseph F. Santner's advice on the anova data analysis, and Allan Gunderson's council and encouragement during the conduct of the mechanical testing. The manuscript was prepared by Mrs. Sally Gardner.

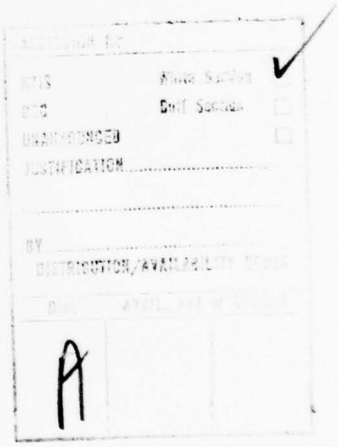

TABLE OF CONTENTS

LIST OF ILLUSTRATIONS

LIST OF TABLES

# SECTION I

# INTRODUCTION

Aluminum alloys used by the Air Force must simultaneously satisfy several requirements to assure that a cost-affordable viable deterrent force is procured. These requirements include high tensile strength, good corrosion resistance, high fracture toughness, and good fatigue properties. All are equally important if new systems are to be cost-affordable. These properties are not only influenced by the alloy chosen, but also by the processing sequence used to fabricate the component, be it cast, forged, extruded or machined from wrought plate/sheet. Each of these material processes produce different grain textures and precipitate dispersions within the grains. Work has been in progress at the Air Force Materials Laboratory to systematically study the relationship between the required properties and the precipitates commonly found in wrought aluminum plate.[1,2,3]

Generally, the precipitates are classified into three types: constituent particles, dispersoid particles, and hardening particles. They are classified in this manner, as they appear in this order during the processing sequence. The constituent particles precipitate from solid solution during the cooling of the ingot. Thus, they are thermodynamically the most stable. From the practical point of view subsequent processing will have little effect on changing the size of these particles, though extensive mechanical working can change their distribution somewhat. These particles are iron and silicon rich, having incoherent interface with the matrix, and ranging in size from 5 to 30 μm. The dispersoid particles precipitate from solid solution during the

homogenizing solution treatment of the ingot. This temperature ranges from 920°F (493°C) for 2024 to 880°F (471°C) for 7075. These particles are chromium and zirconium rich ranging in size from 0.5 μm to 10 μm. The hardening particles are thermodynamically the least stable particles as they can precipitate from the solid solution at room temperature. They range in size from 50 Å (5 nm) to 5000 Å (0.5 μm), having either coherent or incoherent interfaces. These particles are primarily responsible for the high strengths exhibited by the 2000 and 7000 series alloys which are used in aerospace alloys. The copper rich precipitates are found in the 2000 series alloys while the zinc rich precipitates are found in the 7000 series alloys.

The mechanism of ductile fracture has been envisioned as a two step process.[4] The first step involves the nucleation of voids at the macro-inclusions, i.e., inclusions ≥1 μm diameter. The second step is the coalescence of the microcracks by the formation of shear bands between the macroinclusions. Previous work[5] sponsored by the Air Force Materials Laboratory has demonstrated that a high purity in 2000 or 7000 series aluminum alloys dramatically improves the strength vs toughness trend lines over those of commercially pure 2000 or 7000 series aluminum alloys. The question which was not answered was: at what level of purity does the second step in the ductile fracture process become the rate controlling process? It is the purpose of this report to examine this question which has important economic consequences. By specifying higher purity alloys such as 7475 and 7175, cost penalties are incurred. The level of purity below which fracture toughness cannot be improved by this technical approach must be determined.

## SECTION II

## EXPERIMENTAL

### 1. MATERIALS

In order to systematically study the effects of constituent, dispersoid, and hardening particles in wrought aluminum plate, a series of alloys was obtained based on the composition of 7075. To study the effects of constituent particles, five different combined purity levels of iron and silicon were used ranging from 0.03 w/o to 0.3 w/o with the ratio of iron to silicon being held constant at two. For identification purposes, they are labeled "A" through "E" with the most pure called "A".

To assess the role of dispersoid particles, and their interaction with the iron and silicon, both chromium and zirconium are separately added to each of the five purity level alloys for a total of ten different alloys. For identification purposes, a second digit is added. "Zero" (or no explicit identifier) represents the chromium-bearing alloys while "one" represents the zirconium-bearing alloys. The compositions of these ten alloys are given in Table 1.

Two different heat treatments (T651 and TMP) are used on all ten alloys to study the role of hardening particles. The T651 process involves a 1.5% stretch prior to a 24 hour age at 250$^{o}$F (121$^{o}$C) followed by air cooling. The TMP process used is actually a FTMP according to the nomenclature developed by Waldman, et. al.[6] as it occurs after the final solution treatment. Four hours aging at 250$^{o}$F (121$^{o}$C) and 20 minute age at 325$^{o}$F (163$^{o}$C) precede a 25% reduction by warm rolling to 0.625 in. (1.59 cm)

TABLE 1

ALLOY COMPOSITIONS (WEIGHT PERCENTS)

| Designation | Fe | Si | Zn | Mg | Cu | Ni | Mn | Ti | Cr | Zr |
|---|---|---|---|---|---|---|---|---|---|---|
| A | 0.02 | 0.01 | 5.89 | 2.19 | 1.50 | <.01 | <.01 | .004 | 0.21 | ---- |
| B | 0.05 | 0.02 | 5.91 | 2.42 | 1.58 | <.01 | <.01 | .005 | 0.22 | ---- |
| C | 0.08 | 0.04 | 5.93 | 2.39 | 1.60 | <.01 | <.01 | .012 | 0.21 | ---- |
| D | 0.13 | 0.06 | 5.93 | 2.35 | 1.64 | <.01 | <.01 | .012 | 0.21 | ---- |
| E | 0.20 | 0.11 | 5.94 | 2.36 | 1.63 | <.01 | <.01 | .009 | 0.21 | ---- |
| A1 | 0.01 | 0.01 | 5.73 | 2.39 | 1.50 | <.01 | <.01 | .004 | <.01 | 0.12 |
| B1 | 0.04 | 0.02 | 5.68 | 2.31 | 1.51 | <.01 | <.01 | .005 | <.01 | 0.12 |
| C1 | 0.08 | 0.04 | 5.84 | 2.31 | 1.54 | <.01 | <.01 | .006 | <.01 | 0.12 |
| D1 | 0.11 | 0.05 | 6.02 | 2.33 | 1.51 | <.01 | <.01 | .005 | <.01 | 0.12 |
| E1 | 0.20 | 0.09 | 5.98 | 2.45 | 1.52 | <.01 | <.01 | .006 | <.01 | 0.12 |

and a 1.5% stretch. Final aging for two hours at 290°F (143°C) was only used for two of the 10 alloys (B1 and C1) in order to increase their yield strength from unacceptably low values.

Notched tensile specimens were prepared with the tensile axis in both the longitudinal and the long-transverse directions as previous metallographic work[7] verified that grain structure is anisotropic which is commonly found in wrought products.

## 2. MODIFIED NOTCHED TENSILE TEST

Following the proposed ASTM test method for notched tensile tests,[8] 0.5 in. (1.27 cm) diameter specimens were machined to the prescribed geometry. A 50 KIP capacity Instron tensile test machine was used with one universal joint directly threaded into each end of the specimen. With this configuration the measured percent bending stress for a 0.5 in. (1.27 cm) diameter steel specimen was consistently below 10% at 30 KSI (207 MPa) stress level. In addition to measuring the load at failure, the specimen elongation was monitored by means of a ½ in. (1.27 cm) clip-on extensometer. Since the notch cross section area is half that for overall specimen, with a $K_t$ of 11, the measured deformation is approximately that experienced by the material in the notch.[9] The load vs displacement output is recorded on an X-Y plotter. A schematic drawing of a typical test record is given in Fig. 1. The shaded area under the load vs displacement curve is used to calculate the "plastic energy per unit area". This approach assumes that the maximum sustained load by a material prior to failure is in itself insufficient to characterize the fracture toughness of a material which fails by a two-stage process. If ductile fracture in its most general form is a two step process, the specimen elongation is an important measure of fracture toughness. Both the nucleation

of microcracks and their coalescence by a shear band formation involves more deformation than a material which fails before the shearing process becomes fully developed.

## SECTION III

## RESULTS

### 1. NOTCHED TENSILE TESTS

The plastic energy absorbed per unit area, W/A, is plotted as a function of the combined iron and silicon content in Fig. 2 and Fig. 3 for the longitudinal and long-transverse specimens, respectively. Each data point is the average of three test results. The squares are for the specimens heat treated to the T-651 condition while the triangles are used for specimens with the TMP heat treatment. Open symbols connected by dashed lines are used for the chromium-bearing alloys while closed symbols are used for the zirconium-bearing alloys which are connected by solid lines. Although the longitudinal data in Fig. 2 is plotted on a larger scale than the long-transverse data in Fig. 3, all four curves show the same trends. This is interpreted to mean that the dominant micromechanism of fracture is the same for both the longitudinal and the long-transverse directions. This interpretation seems supported by the previous slow bend results on precracked Charpy specimens.[3] Figure 4 is a plot of the total energy absorbed per unit area for the precracked Charpy specimens with the crack propagating in the T-L direction using the same conventions as Figs. 2 and 3. Once again, these four curves show the same trends as in the notched tensile test.

The trends which should be noted are the following. With increasing purity, the chromium-bearing alloys (dashed lines) increase their absorbed energy. This is not the case for the zirconium-bearing alloys (solid lines). Beyond a certain purity level, increasing purity does not increase but actually decreases the fracture toughness. The purity level above which the fracture

toughness does not continue to increase is a function of the heat treatment for the zirconium-bearing alloys. In a T651 condition a combined iron and silicon content of less than 0.12 w/o does not improve the fracture toughness; while in the TMP condition, this value is cut in half (0.6 w/o Fe+Si).

Above the critical iron and silicon purity levels, the zirconium alloys have a larger fracture toughness than the chromium alloys of the same heat treated condition. Below the critical iron and silicon purity levels, the fracture toughness advantage found in the zirconium alloys is lost. Finally, the TMP alloys gave the highest observed values of absorbed energy. Only the highest purity chromium-bearing alloy (0.03 w/o Fe+Si) in the T651 gave absorbed energy values approaching that found in the less pure TMP chromium and zirconium alloys (0.12 w/o Fe+Si).

## 2. FRACTOGRAPHY

Since all four curves in Figs. 2, 3 and 4 displayed the same trends, the fractographic studies were limited to the notched round transverse specimens based on the composition of 7075 (Fig. 3). This subpopulation was chosen as these specimens failed in a single mode of crack opening (Mode I) rather than a dual mode found in three point bending. In addition, the interaction between the constituent particles (Fe, Si) and the dispersoid particles (Cr, Zr) should be more obvious in fractures where the constituent particles would normally dominate the micromechanism of failure.

Figure 5 shows the typical fracture surfaces for the chromium-bearing alloys in the T651 condition. The absorbed energy of these specimens is represented by open squares in Figs. 2, 3 and 4. It is clear that a large number of 2-4 μm size second phase particles is nearly homogeneously distributed throughout the fracture surface of the least pure alloys (Fig. 5c).

However, there are discrete patches of the fracture surface which are either smooth or have a coarse texture. The intermediate purity alloy (Fig. 5b) has a smaller area fraction of regions containing the 2-4 μm size particles. These regions are replaced by either the smooth or coarse textured areas noted in the least pure alloy. The most pure alloy (Fig. 5a) has an inhomogeneous distribution of regions containing the 2-4 μm size particles. These regions are separated by areas of the coarse texture with no smooth areas as found in the other two alloys. In all three alloys, the coarse textured areas separating the regions containing the 2-4 μm size particles are elongated parallel to the plate surface. In addition, 1000X magnification fractographs of the coarse textured areas show approximately 1.0 μm sized ductile dimples not distinguishable in Fig. 5.

Figure 6 shows the typical fracture surfaces for the zirconium-bearing alloys in the T651 condition. The absorbed energy of these specimens is represented by closed squares in Figs. 2, 3 and 4. Like the chromium-bearing alloys in Fig. 5, the area fraction of regions containing the 2-4 μm sized particles increases with increasing iron and silicon content. These regions are also elongated parallel to the plate surface. Unlike the chromium-bearing alloys in Fig. 5, there are no coarse textured areas containing the finer 1 μm sized ductile dimples at 1000X magnification.

Figure 7 shows the typical fracture surfaces for the chromium-bearing alloys in the TMP condition. The absorbed energy of these specimens is represented by open triangles in Figs. 2, 3 and 4. Approximately two-thirds of the 0.12 w/o Fe+Si alloy's fracture surface (Fig. 7b) is composed of elongated macrodimples (≈20 μm x ≈40 μm) which are elongated parallel to the plate surface. These are formed from a number of 2-4 μm sized particles acting

in tandem. Roughly the remaining third of the fracture surface contains the previously mentioned coarse textured areas. The higher purity alloy (Fig. 7a) generally does not show the macrodimples. Its surface contains nearly equal areas of dimples initiated by the 2-4 μm sized particles and the coarse textured areas which 1000X magnification fractographs show to be approximately 1.0 μm diameter ductile dimples.

Figure 8 shows the typical fracture surfaces for the zirconium-bearing alloys in the TMP condition. The absorbed energy of these specimens is represented by closed triangles in Figs. 2, 3 and 4. Like the lower purity chromium bearing alloys, elongated macrodimples (≈20 μm x ≈40 μm) initiated by several 2-4 μm diameter particles acting in tandem are present. However, unlike the chromium-bearing alloys, the coarse textured areas are not present in either the lower or higher purity alloys (0.06 w/o Fe+Si and 0.16 w/o Fe+Si respectively). These areas are replaced by smooth textured areas previously noted for the zirconium-bearing alloys given the T651 heat treatment in Fig. 6. In addition, the elongated macrodimples exist in the higher purity zirconium-bearing alloys while the chromium-bearing alloys did not show this feature.

## 3. ANALYSIS OF VARIANCE

In order to systematically rank the relative importance of the first order, second order and third order interactions, an analysis of variance was performed. Again, for the reasons outlined in paragraph III. 2, the transverse W/A values were used in this analysis. Table 2 summarizes the results for this type of analysis. The first column lists the combinations by which the three variables can influence the measured W/A. The next five columns lists the degrees of freedom (df), the sums of the squares (SS), the mean square (MS), the ratio of the seven combinations each with the error mean square (F), and finally the critical value (CV). The critical value was chosen to be at the 95% confidence

TABLE 2

ANOVA TABLE FOR TRANSVERSE W/A

| SOURCE OF VARIATION | df | SS | MS | F | CV* |
|---|---|---|---|---|---|
| $T_t$(heat treatment) | 1 | 289,537 | 289,537 | 98.58 | 4.08 |
| $D_d$(dispersoid) | 1 | 14,853 | 14,853 | 5.06 | 4.08 |
| T·D | 1 | 20,093 | 20,093 | 6.84 | 4.08 |
| $P_p$(purity level) | 4 | 541,975 | 135,494 | 46.13 | 2.61 |
| T·P | 4 | 196,502 | 49,126 | 16.73 | 2.61 |
| D·P | 4 | 96,237 | 24,059 | 8.19 | 2.61 |
| P·D·T | 4 | 10,963 | 2,741 | 0.93 | 2.61 |
| $\varepsilon_{e(t,d,p)}$ | 40 | 117,487 | 2,937 | 1 | - |

*$F_{.95}(1,40)$ or $F_{.95}(4,40)$ i.e. 4.08 or 2.61

† The Yates Method of analysis used to obtain the ANOVA table is discussed by Charles R. Hicks in "Fundamental Concepts in the Design of Experiments" (Chicago; Holt, Rinehart, and Winston, 1965).

level. It is clear that there is a large variation in the F ratios. This means, of course, that the various combinations of heat treatment (T), dispersoid type (D), and purity level (P) are not all equally weighed in importance. The sources of variation are plotted on the F axis in Fig. 9 to illustrate the relative importance of the tested variables.

Interestingly, the heat treatment (T), which controls the type and distribution of the small hardening particles (5-500nm) is more important than the amount of constituent particles (w/o Fe+Si) present (P). The interaction between these two variables is the third most important variable controlling the fracture toughness. In order to understand these results, the response surface for the interaction between heat treatment and purity level is given in Fig. 10 which is Fig. 3 replotted by combining the open and closed symbols for both heat treatments. The TMP heat treatment gives the highest values for W/A once the purity exceeds the 0.2 w/o Fe+Si purity level.

## SECTION IV

## DISCUSSION

### 1. CONSTITUENT PARTICLES

The level of purity above which significant increases in fracture toughness can be achieved is strongly dependent upon the dispersoid and hardening particles which control the process of shear band formation between the voids which initially form. This fact is dramatically illustrated in Fig. 10 which compares the TMP processed alloys to those heat treated to the T651 temper. In both instances, the lowest fracture toughness was for the least pure alloys ($\simeq$0.30 w/o Fe+Si). To double the toughness from this low value, the purity had to be increased by a factor of two for the TMP processed alloys (0.18 w/o Fe+Si) while a four-fold purity increase (0.07 w/o Fe+Si) was required for the alloys given the T651 heat treatment.

The importance of heat treatment on fracture toughness was also demonstrated by the results of DiRusso, et. al.[10] They tested two laboratory produced 7075 alloys: a commercial purity alloy (0.33 w/o Fe+Si) and a high purity alloy (0.0066 w/o Fe+Si). Each alloy was given two different heat treatments. They named one heat treatment T-A which involves a simple warm aging at 120$^{o}$C for 24 hours (i.e. T6). The second heat treatment involving thermomechanical processing was called T-AHA. It consists of aging at 105$^{o}$C for 6 hours, a 20% reduction by warm rolling at 175$^{o}$C, and a final aging at 120$^{o}$C for 6 hours. Their fracture toughness results are summarized in Table 3. What is most interesting is that the T-AHA heat treated high purity alloy has approximately the same fracture toughness as

TABLE 3

LONG-TRANSVERSE FRACTURE TOUGHNESS PROPERTIES

OF LABORATORY PRODUCED 7075 ALLOYS(1)

| 7075 Alloy With | Fracture Toughness Index, $K_c$ (KSI $\sqrt{in}$) | |
|---|---|---|
| | T-A | T-AHA |
| 0.33 w/o Fe+Si | 40.5 | 27.0 |
| 0.0066 w/o Fe+Si | 57.0 | 37.5 |

(1) DiRusso, E., Conserva, M., Gatto, F. and Markus, M., Met. Trans., 4, (1973), 1133-1144.

the commercial purity alloy having the T-A heat treatment. The absence of constituent particles in itself does not guarantee the optimum fracture toughness is reached for a given alloy. The second stage of shear band formation is the rate controlling process which determines the alloy's fracture toughness.

This conclusion seems to be supported by the results obtained by Hahn and Rosenfield.[11,12] From continuum elastic-plastic analysis,[13] the following failure criterion was proposed from the metallurgical point of view:

$$K_{IC} \simeq \sqrt{2\left(\frac{\pi}{b}\right)^{1/3} \sigma_y E \cdot D}\ f_c^{-1/6} \qquad (1)$$

where $f_c$ is the volume fraction of cracked particles while their diameter is D. As pointed out by Hahn and Rosenfield, while equation (1) predicts the right order of magnitude for $K_{IC}$ with experimental observation, a fundamental contradiction exists between the model and the experimental results. The model predicts for a constant modulus and volume fraction of cracked particles, the toughness will increase with increasing yield strength (i.e. $K_{IC} \propto \sqrt{\sigma_y}$). The experimental results given in Fig. 11 show that as the yield strength increases from (0.0057) E to (0.0085) E, the fracture toughness decreases at a constant volume fraction of cracked particles. They attribute the loss of toughness to plastic instabilities associated with narrow bands of inhomogeneous slip linking the macrovoids. This shear band formation is controlled by the particles which we have called hardening and dispersoid particles.

## 2. DISPERSOID AND HARDENING PARTICLES

The hypothesis that the dispersoid and hardening particles in aluminum alloys play an equally important role for determining a material's fracture

toughness is not new. Experimental evidence was presented by Broek.[14] His ideas are consistent with the two-step process mechanism for ductile failure presented by Thompson and Weihrauch[4] and therefore are useful to explain the experimental results. In Broek's study of thirteen commercial aluminum alloys, both small dimples as well as large voids were observed on the fracture surfaces. The fractographic analysis given in Section III. 2 makes the same observation. Thus the required presence of a bimodal distribution of dimple size on a fracture surface is fulfilled.

Broek's study of dimple profiles found that the dimples ranging in size from 0.2 to 2.0 μm were relatively shallow holes. Thus, if shear band formation would be the second step for ductile fracture mechanism, shallow dimple profiles are expected. While no direct measurements of dimple profiles were made in the present study, indirect evidence suggests that shear band formation occurred.

In the chromium-bearing alloys, the fractographs clearly showed dimples with these areas described as "being coarse textured" in Figs. 6 and 8. These same coarse textured regions were absent in the zirconium-bearing alloys in Figs. 5 and 7. This does not mean that a much finer sized ductile dimple does not exist. Fractographic evidence published by Santner and Fine[15] recently demonstrated that a featureless "rock candy" appearing grain boundary fracture can indeed be a ductile dimple failure at sufficiently high magnification. Their work on a high purity binary Al-3.6 w/o Cu alloy identified a 0.2 μm sphere-like precipitate in the grain boundary responsible for this failure mode.

Profile shots of the high purity (0.02 w/o Fe+Si) and low purity (0.31 w/o Fe+Si) specimen, shown in Fig. 12, also supports the hypothesis that the zirconium-bearing alloys failed by shear band formation. It is interesting

to note that in Fig. 12a, approximately half of the fracture surface does not have a well-developed zig-zag profile as described by Beachem and Yoder.[16] The average fracture energy, W/A, for this specimen is about half of that measured for the higher purity alloy pictured in Fig. 12b (48 lb/in vs 94 lb/in). This suggests that the second stage of shear band formation is primarily responsible for the increase in the alloy's fracture toughness and is responsible for the nonlinear portion of the load-deflection curve schematically drawn in Fig. 1.

This hypothesis was further tested by performing high magnification TEM replica fractography on the zirconium-bearing alloys. The results of this work is summarized in Fig. 13. The top row is for material given for T651 heat treatment while the TMP processed material is on the bottom row. The first column shows the high purity material (Al = 0.02 w/o Fe+Si) while the least pure material (El = 0.29 w/o Fe+Si) is in the last column. In all four cases ductile dimples were observed. For the TMP material the lower magnification permitted observing a bimodal distribution in ductile dimple size. In particular the Al-TMP fractograph shows 0.25 μm diameter ductile dimples. The dimples for the El-TMP fractograph were approximately the same size, only showing more shear for this particular area. The fractographs for the material with T651 temper were taken at a higher magnification. Both have ductile dimples that were approximately 0.50 μm, about twice as large as that found for the corresponding alloys processed by TMP. This TMP appears to have produced a larger number of the small second phase particle sites than the T651 processed material.

The experimental evidence suggests that microvoid coalescence was achieved for both the chromium-bearing and zirconium-bearing aluminum alloys

with a total iron and silicon content of less than 0.2 w/o. The chromium-bearing alloys had clearly visible regions in the shear band containing approximately 1 μm diameter dimples, while this was not the case for the zirconium-bearing alloys. The available evidence (Figs. 12 and 13) suggests that a smaller sized particle is responsible for the shear-band formation in the zirconium-bearing alloys. Moreover, the fact that the TMP alloys out-performed the same alloys given the T651 heat treatment (see Section III. 3) negates the hypothesis that the inclusions alone determine an alloy's fracture toughness. As explained in the introduction, the TMP process cannot substantially affect the size and spacing of the large constituent particles.

## SECTION V

## SUMMARY AND CONCLUSIONS

A modified notched round tensile test which measured the plastic energy per unit area, W/A, is used to measure the relative fracture toughness of ten different aluminum alloys based on the 7075 composition. The fracture toughness ranking for these alloys is the same in the longitudinal and long transverse directions and agrees with the ranking found in precracked Charpy tests.[3] These results suggest that the same micromechanisms are responsible for determining the fracture toughness of all ten aluminum alloys tested having the composition of 7075.

Fractographic analysis clearly indicated a distinct difference in the amount of large voids present with different weight percents of iron plus silicon. In addition, the smaller dimples found between the large voids were different for the chromium-bearing and zirconium-bearing alloys. While the chromium-bearing alloys had dimples on the order of 1.0 μm, similar dimples were not visible in the 500X fractographs of the zirconium-bearing alloys. However, replica TEM fractography showed 0.25 to 0.50 μm dimples were present. The size of these dimples appear to be related to the heat treatment.

The analysis of variance clearly demonstrated that heat treatment which controls the size and distribution of the hardening particles is the most important variable effecting fracture toughness. This then supports the two-stage hypothesized mechanism of ductile fracture. If the fracture toughness were controlled by the amount of iron and silicon present, then one

must conclude the failure is a one-step process or the purity levels are not sufficiently high to insure that the second stage becomes active. The results of this work suggest that at 0.2 w/o Fe+Si, the second stage process of shear band formation becomes significant. Past research has shown that increasing fracture toughness is generally associated with a decrease in yield strength. Generally, fracture toughness is increased by controlling the amount of constituent particles present, while the yield strength is controlled by the type of hardening particles present. Thus, it appears for the first time that the fracture toughness can be increased with no loss in yield strength if the proper heat treatment (which may involve mechanical working) is applied to aluminum alloys with less than 0.2 w/o Fe+Si. Since the hardening particles not only control the yield strength but also the work hardening rate, it makes sense that both factors are important if shear band formation is the rate controlling step for fracture.

Two questions were raised in the introduction. First, at what purity level does the second step in the ductile fracture process become the rate controlling step? Second, is there a purity level beyond which further purity improvements will not produce improved fracture toughness? At any purity level below 0.2 w/o Fe+Si the microstructural variables of dispersoid type (Cr vs. Zr) and heat treatment (TMP vs. T651) produce very different fracture toughness values as reflected in the W/A measure. So 0.2 w/o Fe+Si is the critical purity level. For the Cr-bearing alloys, there is no purity level beyond which further purity improvements will produce improved fracture toughness. However, in the Zr-bearing alloys, it is possible to have no further increase in fracture toughness with increasing purity. The cause for this dilemma is not presently understood.

## REFERENCES


1. "Influence of Iron and Silicon Content on the Tensile Properties of 7X75 and Zr-Modified 7X75 Aluminum Plate", AFML-TR-75-140, July 1975, Air Force Materials Laboratory, WPAFB, OH.

2. "Effect of Iron and Silicon Content on Stress Corrosion Cracking in a Thermomechanically Processed Aluminum Alloy", AFML-TR-75-43, July 1975, Air Force Materials Laboratory, WPAFB, OH.

3. "Effect of Iron and Silicon Content on the Fracture Toughness of 7X75 and Zr-Modified 7X75 Aluminum Plate", AFML-TM-LL-75-10, July 1975, Air Force Materials Laboratory, WPAFB, OH.

4. Thompson, A.W. and Weihrauch, P.F., "Scripta Met", 10, (1976), 205-210.

5. "Program to Improve the Fracture Toughness and Fatigue Resistance of Aluminum Sheet and Plate for Aircraft Applications", AFML-TR-73-224, Sept 1973, Air Force Materials Laboratory, WPAFB, OH.

6. Waldman, J., Sulinski, H. and Markus, H., Met. Trans. 5, (1974), 573-584.

7. Blau, P.J., "Observations on the Distribution of Iron and Silicon Particles in a High-Strength Aluminum Alloy", "Metallographv", 7, (1975), 187-201.

8. 1975 Annual Book of ASTM Standards, Part 10: Metals-Mechanical, Fracture, and Corrosion Testing; Fatigue; Erosion; Effect of Temperature. Proposed Method for Sharp-Notch Tension Testing of Thick High-Strength Aluminum and Magnesium Alloy Products with Cylindrical Specimens, 799-810.

9. Santner, J.S. and Gunderson, A., "Development of a Low Cost Reliable Test to Verify Fracture Toughness of Light Metal Alloys".

10. DiRusso, E., Conserva, M., Gatto, F. and Markus, H., Met. Trans., 4, (1973), 1133-1144.

11. Hahn, G.T. and Rosenfield, A.R., "Metallurgical Fracture Affecting Fracture Toughness of Aluminum Alloys", Presented at the 5th Annual Spring Meeting of TMS/AIME, May 29-June 1, 1973.

12. Hahn, G.T. and Rosenfield, A.R., "Relations Between Microstructure and the Fracture Toughness of Metals", Third International Conference on Fracture, Paper PL-III-211, (1973), Munich.

13. Rice, J.R., Johnson, M.A., Kanninen, M.F., et.al., "Inelastic Behavior of Solids", editors, McGraw-Hill, New York, 1970, p. 641.

14. Broek, D., "A Study on Ductile Fracture", National Aerospace Laboratory, NLR, The Netherlands, NLR-TR-71021U, 1971.

15. Santner, J.S. and Fine, M.E., "Origin of Brittle Intergranular Fatigue Fracture in Warm Aged Al-3.6 w/o Cu", Met. Trans., 7A, April 1976, 601-604.

16. Beachem, C.D. and Yoder, G.R., "Elastic-Plastic Fracture by Homogeneous Microvoid Coalescence Tearing Along Alternating Shear Planes", Met. Trans., 4, April 1973, 1145-1153.

## FRACTURE ENERGY IN NOTCH-ROUND TENSILE SPECIMEN

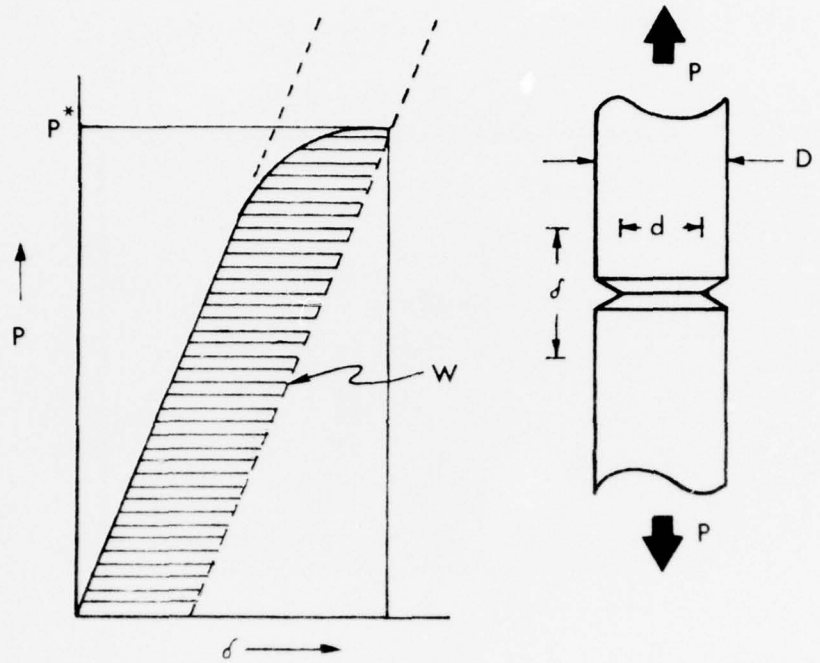


$$K_c^* = \frac{P^*}{D^{3/2}} \left(1.72 \frac{D}{d} - 1.27\right)$$

$$NTS = \frac{P^*}{A}, \text{ WHERE } A = \pi \left(\frac{d}{2}\right)^2$$

$$\frac{W}{A} = \text{'PLASTIC ENERGY' PER UNIT AREA}$$

Figure 1. Schematic of Typical Load vs. Extensometer Displacement Output from a Notched Round Tensile Test.

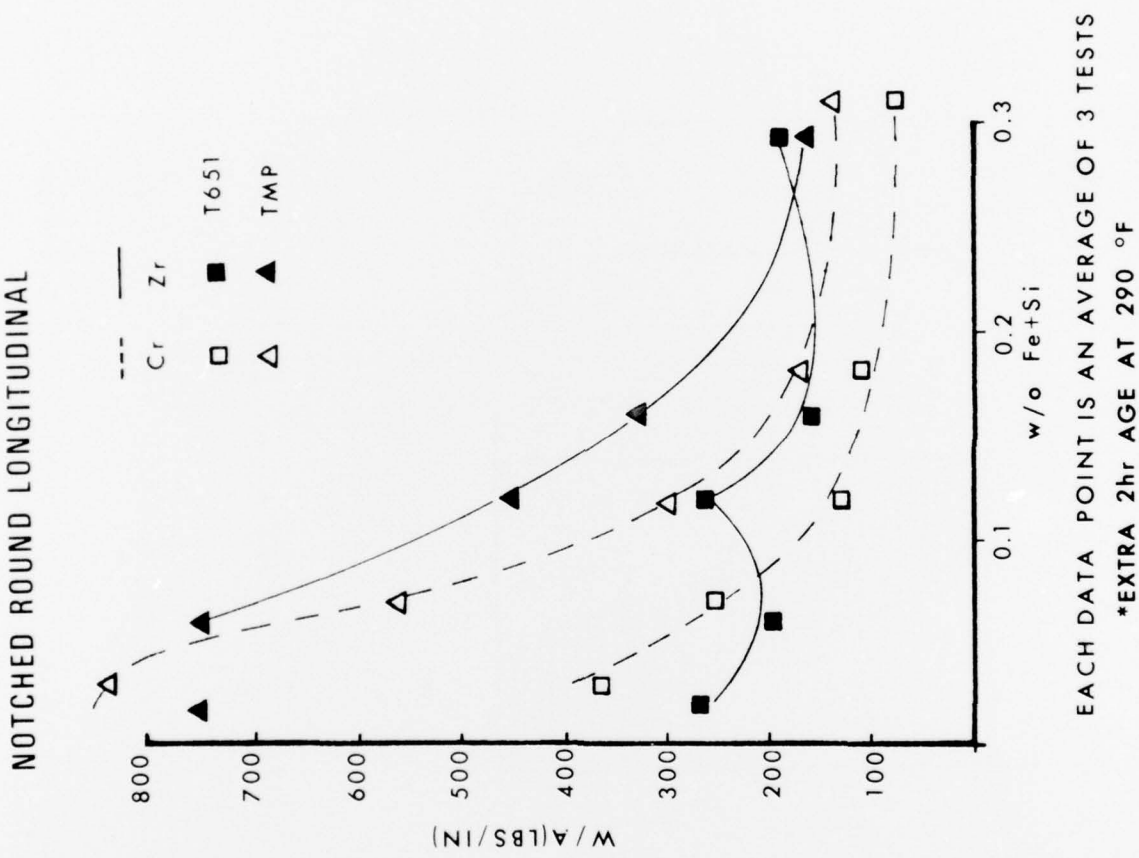


Figure 2. W/A vs. w/o Fe+Si for Notched Round Longitudinal Specimens of 7X75 Alloys with T651 and TMP Heat Treatments.

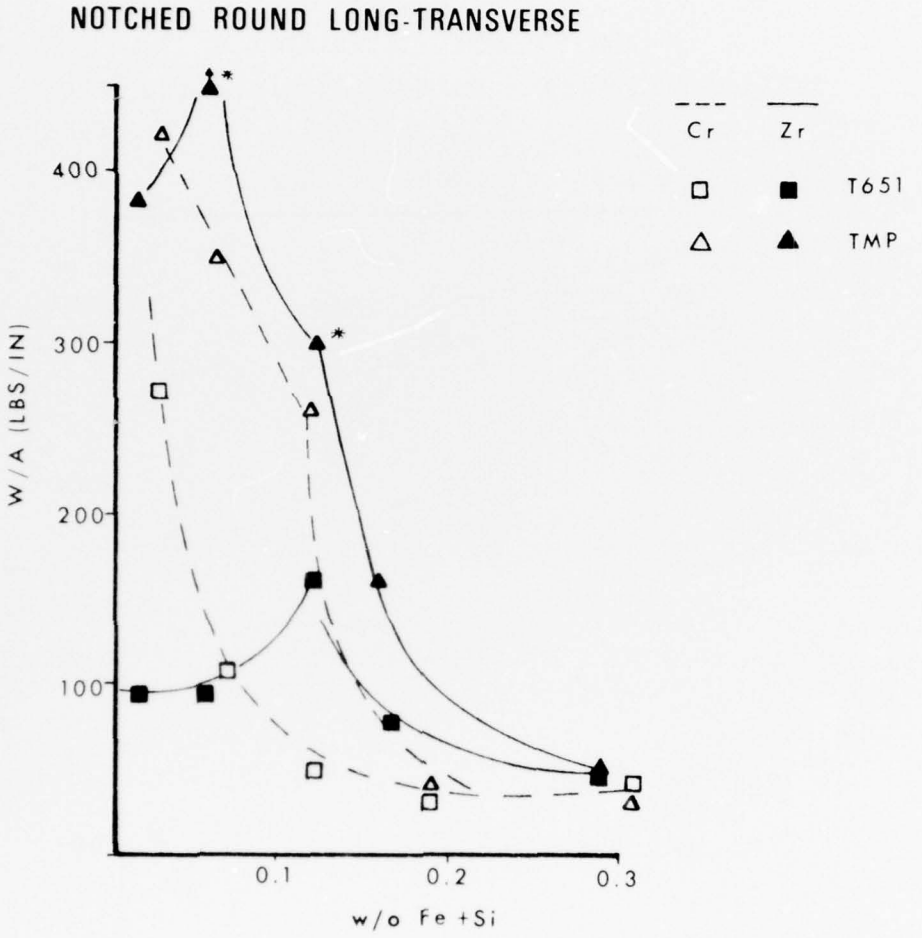


Figure 3. W/A vs. w/o Fe+Si for Notched Round Transverse Specimens of 7X75 Alloy with T651 and TMP Heat Treatment.

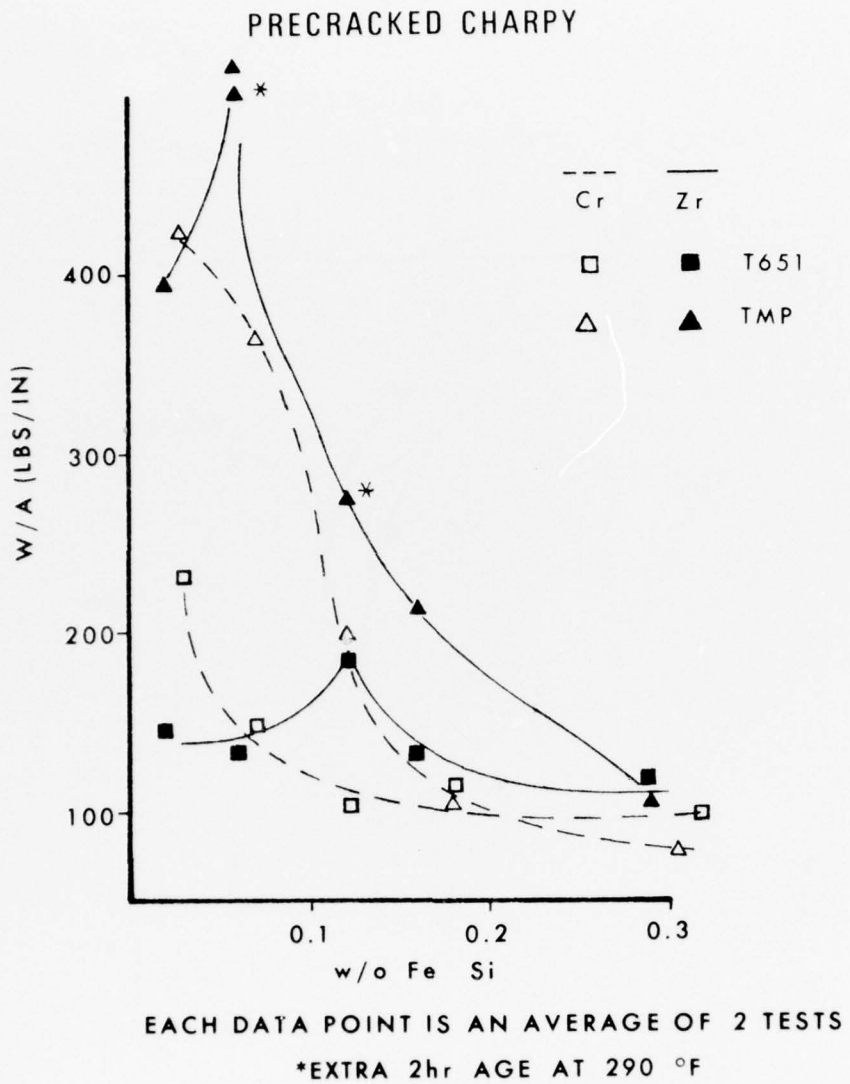


Figure 4. W/A vs. w/o Fe+Si for Pre-Cracked Charpy Transverse Specimens of 7X75 Alloy with T651 and TMP Heat Treatments.

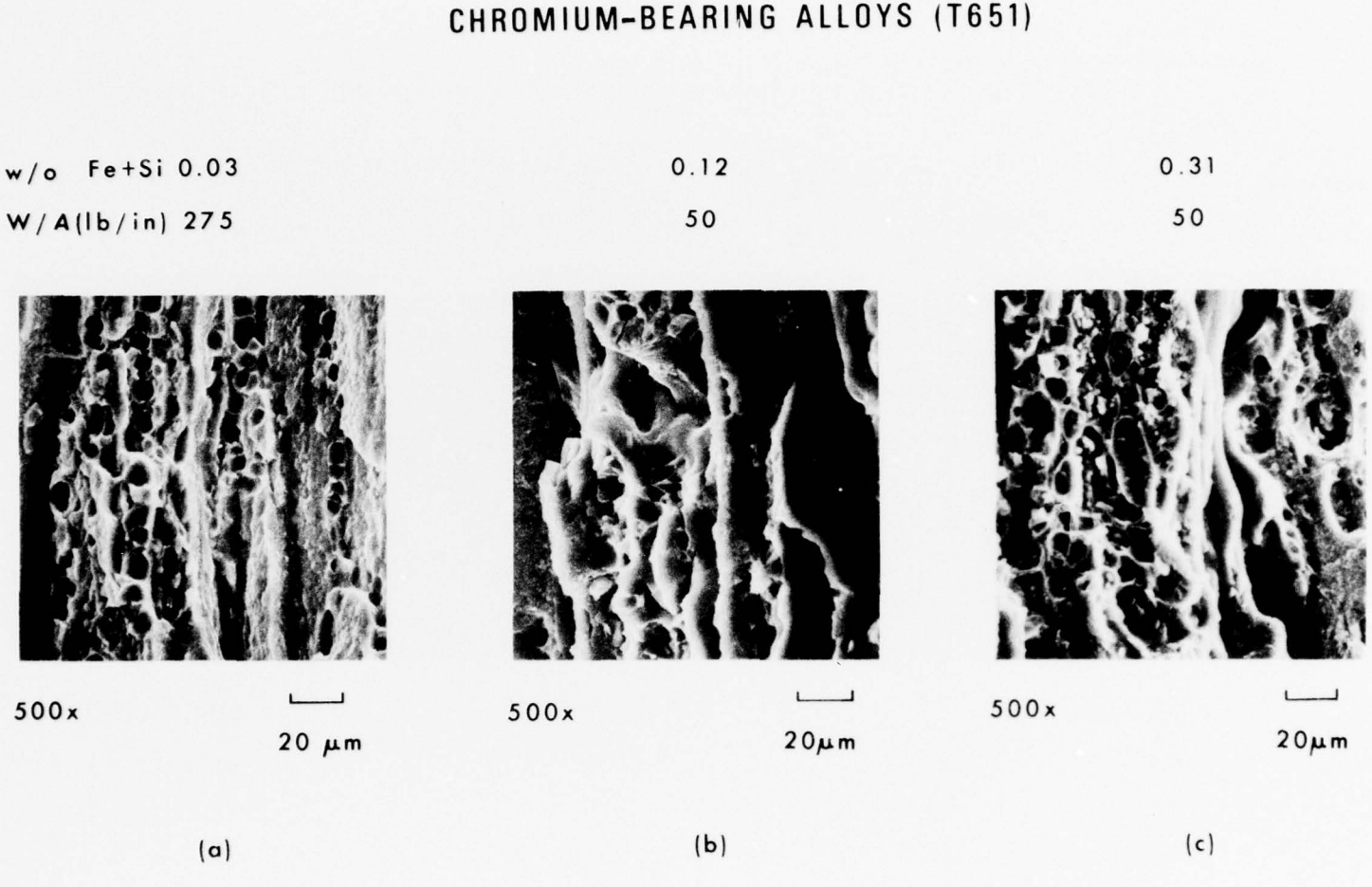


Figure 5. Typical Fracture Areas of Chromium Bearing Alloys in the T651 Condition, (a) 0.03 w/o Fe+Si, (b) 0.12 w/o Fe+Si, (c) 0.31 w/o Fe+Si. Magnification: 500X

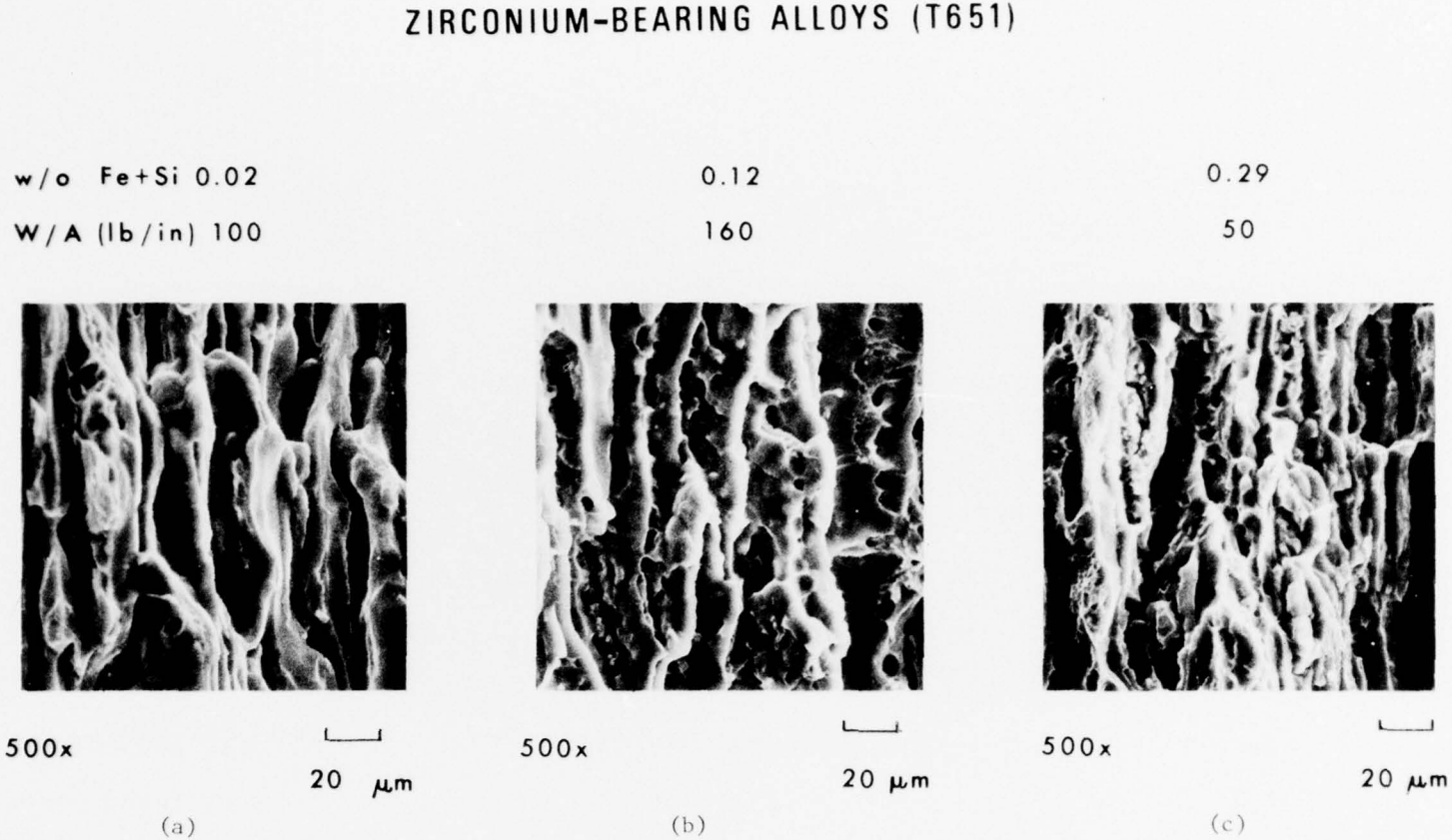


Figure 6. Typical Fracture Areas of Zirconium Bearing Alloys in the T651 Condition, (a) 0.02 w/o Fe+Si, (b) 0.12 w/o Fe+Si, (c) 0.29 w/o Fe+Si. Magnification: 500X.

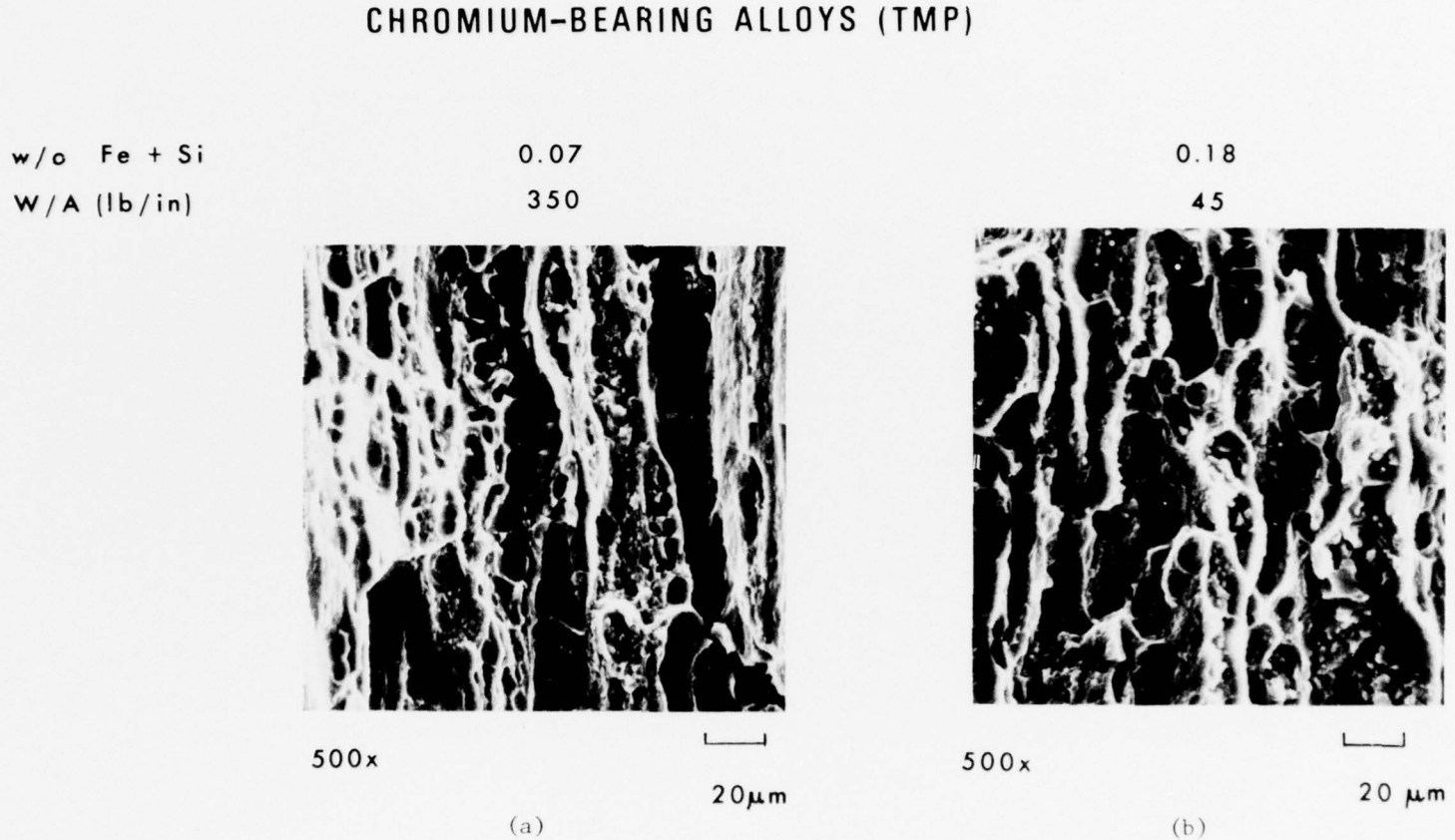


Figure 7. Typical Fracture Areas of Chromium Bearing Alloys in the TMP Condition, (a) 0.07 w/o Fe+Si, (b) 0.18 w/o Fe+Si. Magnification: 500X.

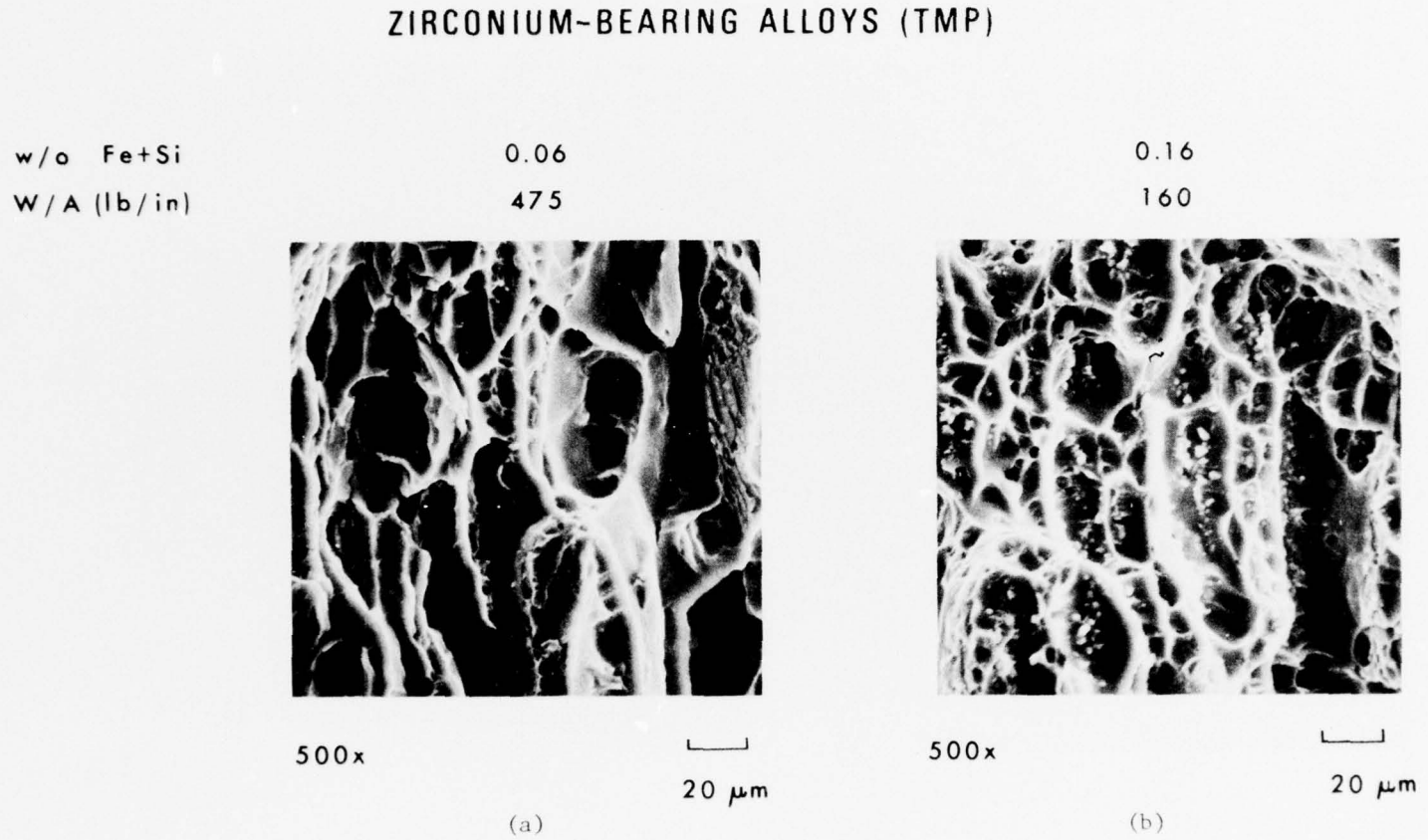


Figure 8. Typical Fracture Areas of Zirconium Bearing Alloys in the TMP Condition, (a) 0.06 w/o Fe+Si, (b) 0.16 w/o Fe+Si. Magnification: 500X.

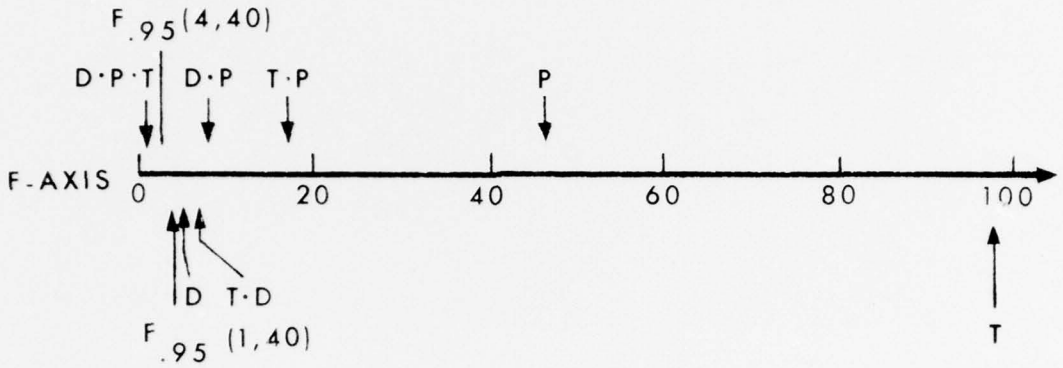


Figure 9. Rank Order of Variables Based on F Distribution.

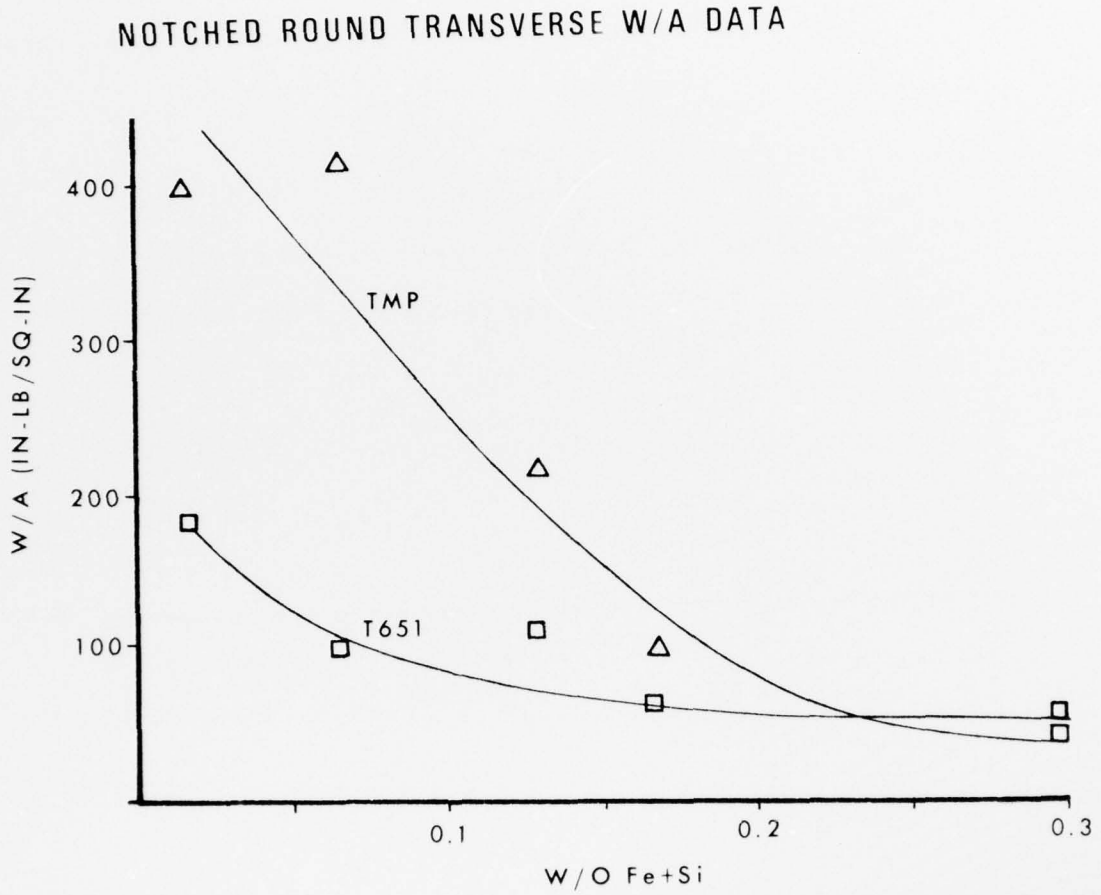


Figure 10. W/A vs. w/o Fe+Si for Notched Round Transverse Specimens of 7X75 Alloys with T651 and TMP Heat Treatments. Each Data is the Average of Six Test Results.

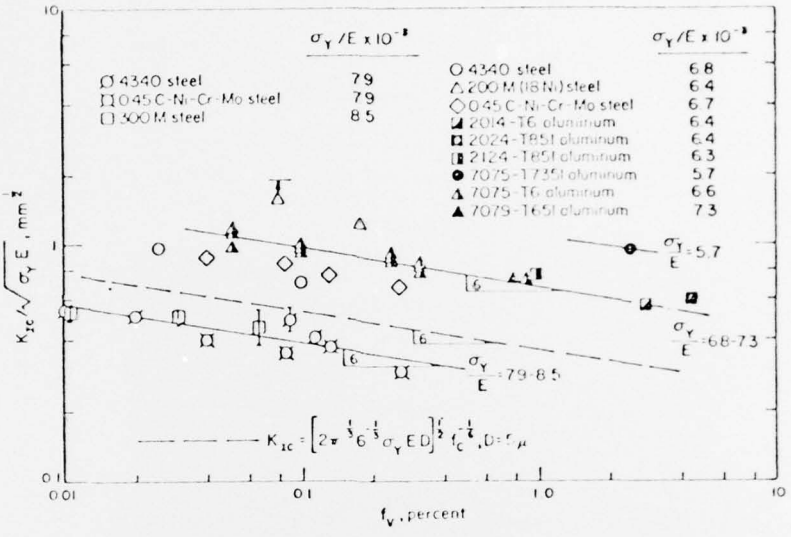


Figure 11. Hahn and Rosenfield Comparison of Experimental Results with the Rice-Johnson Model for Ductile Failure.

7.6X 4mm

(a)

7.6X 4mm

(b)

Figure 12. Fracture surface profile of zirconium bearing alloys tested in the transverse direction (original plate surface perpendicular to plane of photograph), (a) 0.29 w/o Fe+Si, (b) 0.02 w/o Fe+Si.

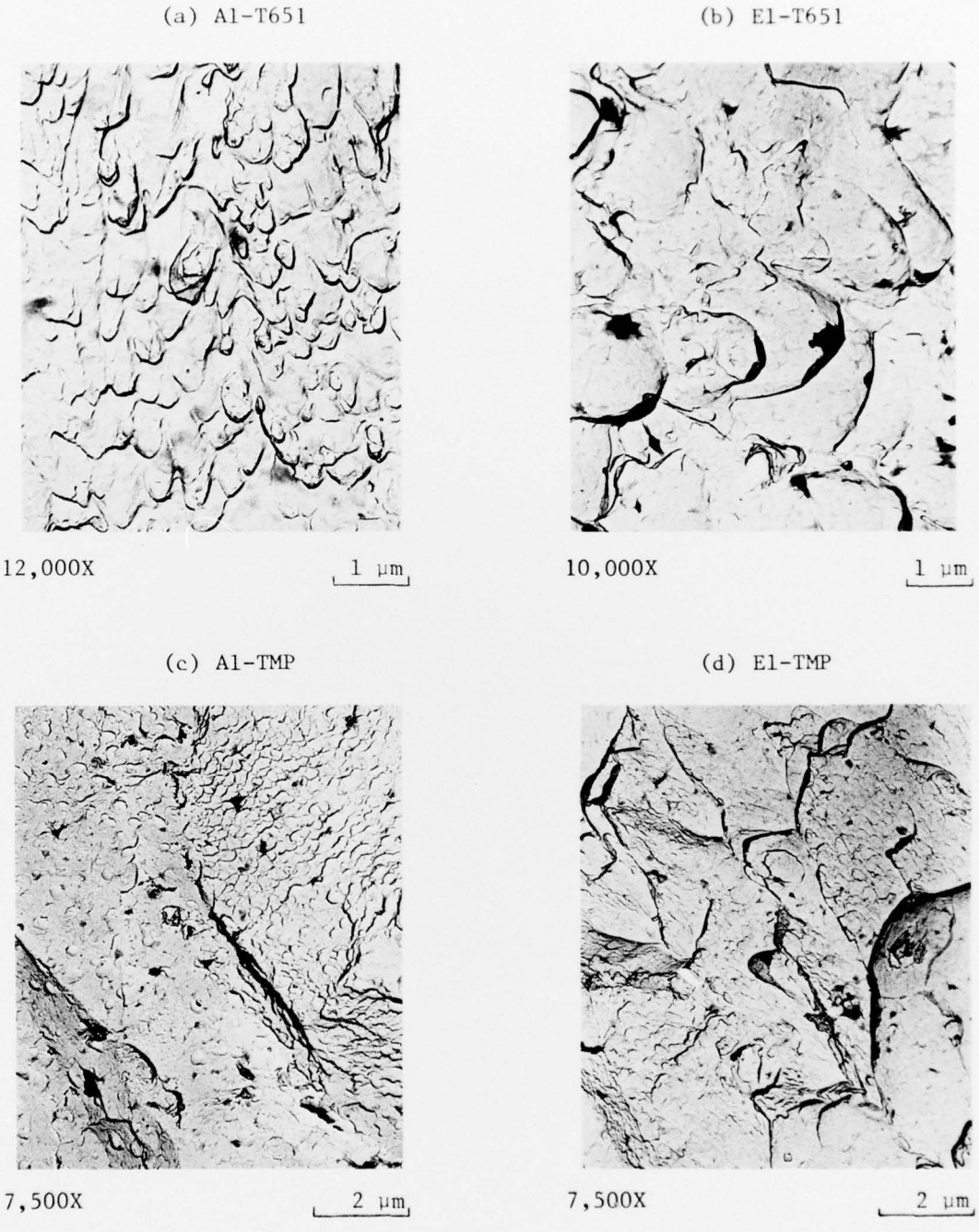


Figure 13. Replica TEM Fractographs of Zirconium-Bearing Alloys Showing the Small Ductile Dimples Formed by the Dispersoid and Hardening Particles. (a) A1-T651, (b) E1-T651, (c) A1-TMP, (d) E1-TMP.



☆ U. S. GOVERNMENT PRINTING OFFICE: 1977 — 757-001/419